A plasma chemistry model for H_2/SiH_4 mixtures used in PECVD processes

Physica Scripta

PAPER

A plasma chemistry model for H_2/SiH_4 mixtures used in PECVD processes

Vladimir Sushkov*, Lazhar Rachdi and Marc Hofmann

Fraunhofer Institute for Solar Energy Systems, Freiburg, Germany

* Author to whom any correspondence should be addressed.

E-mail: v.sushkov78@gmail.com

Keywords: plasma, chemistry, model, H_2/SiH_4, mixtures, PECVD

OPEN ACCESS

RECEIVED
12 August 2022

REVISED
22 February 2023

ACCEPTED FOR PUBLICATION
3 March 2023

PUBLISHED
21 April 2023

Abstract

Plasma chemical processes in H_2/SiH_4 discharges are critically reviewed. A model set of reactions is proposed which includes temperature and pressure-dependent reaction rates and describes Si_yH_x ($y \leqslant 3$) chemistry. Using a 2D fluid plasma simulator, the model has been tested under three different set of operating conditions. First, it has been validated against the experimental benchmark data (Horvath and Gallagher (2009) *J. Appl. Phys.* **105**, 13304). Based on considerations of atomic hydrogen content, the branching of SiH_4 dissociation channels and the H surface loss probability have been defined more accurately. Then, simulations have been also performed for the plasma source of a PECVD tool from Meyer Burger Germany. A very good agreement between the computed and experimentally determined deposition rates can be stated.

Introduction

Thin films of hydrogenated amorphous silicon a-Si:H are widely used in photovoltaic industry to produce efficient solar cells [1]. In order to become more competitive, the industrial PECVD processes producing these layers require optimization in terms of film properties, uniformity, high throughput.

Detailed understanding of the physics and chemistry behind the deposition process is indispensable in realizing these goals. Comprehensive modelling and simulation of a deposition device can be extremely helpful in achieving such understanding.

A lot has been already done in the research field of SiH_4/H_2 discharges. Back in the end of the 80s, the simulation studies by M. Kushner [2, 3] laid the foundation in terms of full-scale modelling. The works by Perrin and co-authors [4–9] advanced the field further, unraveling various aspects of gas-phase and surface processes and providing data needed for modelling purposes. The summarizing work [7] offers compilation and critical review of the knowledge available in the mid-90s. After that, research in the field of a-Si:H deposition continued, but the focus shifted to plasma-surface interaction due to the rise of extensive computing. Such methods like molecular dynamics and kinetic Monte Carlo proved very useful in studying the details of the film growing mechanisms and radical-surface interactions, just to cite a couple of examples [10, 11].

Despite all the progress, still lacking in the literature is a conclusive plasma chemistry model with consistent pressure- and temperature-dependent rate constants and an appropriate description of Si_2H_x radicals.

The present study seeks to fill the gap. The focus is on thorough compilation of reaction set and on updating the rate constants by making use of the literature which is beyond the scope of [7].

The paper is organized as follows. Following *Introduction* section, *Plasma Chemistry Model* presents full lists of species, reactions, and constants. Some crucial reaction pathways are critically reviewed. The described set of reactions has been used within the the fluid simulator Quantemol-VT, that is also briefly introduced. In *Experiment* section, we describe a-Si:H deposition performed by a capacitively coupled radio frequency plasma source in an industrial-type inline PECVD tool (Meyer Burger MAiA). This section also gives the design and operation of the TIMS experiment [12] whose data are used to validate our model. In *Results and Discussions*, a validation of our model is performed for three different cases of discharge conditions. The simulated and

Table 1. List of the species employed in the model. The choice of β, s is discussed later in the text.

	Surface loss probability β	Sticking coefficient s	References
H_2	0	0	
H	0.2–1.0	etching, see text	[13]
SiH_4	0	0	
SiH_3	0.26	0.09	[4]
SiH_2	0.7	0.7	[10]
SiH	0.95	0.95	[7]
Si	1	1	[7]
Si_2H_2	0.5	0.1	[12]
Si_2H_3	0.95	0.95	[14]
Si_2H_4	0.4	0.1	[14]
Si_2H_5	0.26	0.09	[14]
Si_2H_6	0	0	
Si_3H_x	0	0	
H^+	1	0	[7]
H_2^+	1	0	[7]
H_3^+	1	0	[7]
SiH_3^+	1	1	[6]
SiH_2^+	1	1	[6]
SiH_3^-	1	0	
e	1	0	

experimental values are compared for the following sets of parameters: (1) dilution ratio $R_0 = 0$, pressure p = 0.3 Torr and temperature T = 300 K; (2) $R_0 = 40$, p = 1.5 Torr, T = 300 K; (3) $R_0 = 4.5$, p = 0.225 Torr, T = 523 K. In cases (1) and (2), we compare the radical fluxes onto the surface with those obtained in work [12]. In case (3), our model computes the deposition rate which is correlated with the experimentally obtained in MAiA tool. In *Conclusion*, the essential points are recapitulated. This is followed by acknowledgments in the end.

Plasma chemistry model

Introduction

The goal of this work is to develop a model for H_2/SiH_4 discharges which is appropriate in the range of operating conditions 0.1 Torr < p < 1.5 Torr and 300 K < T < 700 K. This means that the p and T dependencies of the reaction rates must be considered whenever possible. The film deposition under these conditions is essentially determined by the fluxes of neutral radicals of small Si-atom numbers [3]. Accordingly, our plasma model involves rather detailed chemistry of SiH_x and Si_2H_x species. Si_3H_x molecules are represented by a single lumped state, which concept is briefly discussed in the end of this section. The relative contribution of ion fluxes is usually much smaller but may become more significant approaching the lower end of the pressure range [5]. Ion-neutral reactions would not generally change the total number of ions, so that there is no need in overly detailed volumetric ion chemistry. Therefore, only most principal ions are retained in the model, which are the primary products of the electron impact ionization of the precursor gases.

Species and reactions used in the model

All the species and reactions between them are summarized in tables 1–3.

In total, there are 20 species in the model which are listed in table 1. The radicals and ions are supplied with respective surface loss probability β and sticking coefficient s, following the notation from [7]. While β describes the total losses on a boundary, sticking coefficient gives the portion of the incident flux which gets incorporated into the film, thus contributing to the film growth. The recombination coefficient γ represents the probability to form a stable volatile product, so that holds $\beta = s + \gamma$. The choice of these probabilities is discussed in the end of this section.

The starting point of the plasma chemistry is the dissociation by electron impact, see reactions R1-R4 in table 2. For all the importance of the dissociation, there is no clarity on the branching of specific channels. There is common agreement that the main channels are R1 and R2, yet the ratio between them R1/R2 takes values in the wide range between 8.5 and 0.2 (e.g. [2]). This last extreme point R1/R2 = 0.17/0.83 is popular in the literature on modelling. It is based on a single experimental evidence, originating from the direct photolysis of silane by 147 nm radiation [30], and it was suggested afterwards that this might also relate to the dissociation by

Table 2. List of electron-impact reactions.

R1	$SiH_4 + e \rightarrow SiH_3 + H + e$	[15]
R2	$SiH_4 + e \rightarrow SiH_2 + H + H + e$	[15]
R3	$SiH_4 + e \rightarrow SiH + H_2 + H + e$	[15]
R4	$SiH_4 + e \rightarrow Si + H_2 + H_2 + e$	[15]
R5	$SiH_4 + e \rightarrow SiH_3^+ + H + e + e$	[3]
R6	$SiH_4 + e \rightarrow SiH_2^+ + H + H + e + e$	[3]
R7	$SiH_4 + e \rightarrow SiH_3^- + H$	[3]
R8	$SiH_3 + e \rightarrow SiH_2 + H + e$	[15]
R9	$SiH_3 + e \rightarrow SiH_3^+ + e + e$	[15]
R10	$Si_2H_6 + e \rightarrow SiH_4 + SiH_2 + e$	[16]
R11	$Si_2H_6 + e \rightarrow Si_2H_4 + H + H + e$	[16]
R12	$Si_2H_6 + e \rightarrow SiH_3^+ + SiH_3 + e + e$	[16]
R13	$H_2 + e \rightarrow H_2^+ + 2e$	[17]
R14	$H_2 + e \rightarrow H^+ + H + 2e$	[17]
R15	$H_2 + e \rightarrow H + H + e$	[17]
R16	$H + e \rightarrow H^+ + 2e$	[17]
R17	$H_2^+ + e \rightarrow H^+ + H + e$	[17]
R18	$H_2^+ + e \rightarrow H + H$	[18]
R19	$H_3^+ + e \rightarrow H_2 + H$	[19]

Table 3. List of reactions between heavy particles. Si_3H_x stands for Si_3H_5 in R28, Si_3H_7 in R29 and Si_3H_8 in R32.

	Reaction	Rate constant [cm^3/s]	Reference
R20	$SiH_4 + H \rightarrow SiH_3 + H_2$	$1.37 \times 10^{-10} \exp(-1820/T)$	[20]
R21	$SiH_3 + H \rightarrow SiH_2 + H_2$	$3.55 \times 10^{-10} (T/298)^{-0.05} \exp(-77/T)$	[21]
R22	$SiH_2 + H \rightarrow SiH + H_2$	$7.38 \times 10^{-10} (T/298)^{0.07} \exp(-229/T)$	[21]
R23	$SiH + H \rightarrow Si + H_2$	$3.59 \times 10^{-10} (T/298)^{-0.32} \exp(-299/T)$	[21]
R24	$SiH_2 + SiH_4 \rightarrow Si_2H_6$	$4.3 \times 10^{-8}(T/300)^4\exp(-T/44) + + 1.9 \times 10^{-9}(T/300)\exp(-T/93) \times p$ [Torr]	[22, 23]
R25	$SiH_2 + SiH_4 \rightarrow Si_2H_4 + H_2$	$5.15 \times 10^{-12} \exp(-210/T)$	[23]
R26	$SiH_2 + H_2 \rightarrow SiH_4$	3.0×10^{-12}(1-1/(1 + 0.03p[Torr]))	[7]
R27	$SiH + SiH_4 \rightarrow Si_2H_3 + H_2$	the same as for R24	
R28	$Si_2H_3 + SiH_4 \rightarrow Si_3H_x$	2.0×10^{-10}	[7]
R29	$Si_2H_4 + SiH_3 \rightarrow Si_3H_x$	2.0×10^{-12}	[14]
R30	$Si_2H_4 + H \rightarrow Si_2H_5$	5.0×10^{-12}	[14]
R31	$SiH_2 + Si_2H_6 \rightarrow Si_2H_4 + SiH_4$	$3.34 \times 10^{-9}(T/298)^{-2} \exp(-1509/T)$	[24]
R32	$SiH_2 + Si_2H_6 \rightarrow Si_3H_x$	$9.27 \times 10^{-6}(T/298)^{-10.2} \exp(-2565/T)$	[24]
R33	$SiH_3 + SiH_3 \rightarrow SiH_4 + SiH_2$	8.25×10^{-11}	[25]
R34	$SiH_3 + SiH_3 \rightarrow Si_2H_4 + H_2$	2.0×10^{-11}	[25]
R35	$Si_2H_6 + H \rightarrow Si_2H_5 + H_2$	$1.15 \times 10^{-12} (T/298)^{1.8}\exp(-10/T)$	[26]
R36	$Si_2H_6 + H \rightarrow SiH_3 + SiH_4$	$1.7 \times 10^{-12} (T/298)^{1.6}\exp(-630/T)$	[26]
R37	$Si_2H_6 + SiH_3 \rightarrow Si_2H_5 + SiH_4$	$4 \times 10^{-10} \exp(-2500/T)$	[7]
R38	$Si + SiH_4 \rightarrow Si_2H_2 + H_2$	3.5×10^{-10}	[27]
R39	$H_2 + H \rightarrow H + H + H$	$4.67 \times 10^{-7}(T/298)^{-1} \exp(-55000/T)$	[28]
R40	$SiH_3^- + H_3^+ \rightarrow SiH_4 + H_2$	1.2×10^{-10}	calcul. from [7]
R41	$SiH_3^- + SiH_2^+ \rightarrow SiH_3 + SiH_2$	1.3×10^{-10}	
R42	$SiH_3^- + SiH_3^+ \rightarrow SiH_3 + SiH_3$	1.2×10^{-10}	
R43	$SiH_4 + H_2^+ \rightarrow SiH_2^+ + H_2 + H_2$	2×10^{-10}	[29]
R44	$SiH_4 + H_2^+ \rightarrow SiH_3^+ + H_2 + H$	6.22×10^{-10}	[29]
R45	$SiH_4 + H_3^+ \rightarrow SiH_3^+ + H_2 + H_2$	5.16×10^{-10}	[29]
R46	$H_2 + H_2^+ \rightarrow H_2 + H^+ + H$	$1 \times 10^{-8} \exp(-84100/T)$	[28]
R47	$H_2 + H_2^+ \rightarrow H_3^+ + H$	$3.22 \times 10^{-10} \exp(-21856/T)$	[28]
R48	$H_2 + H^+ \rightarrow H_2^+ + H$	2.1×10^{-9}	[28]

electron impact. In view of the lack of experimental and theoretical support for this branching value, we prefer to use a more moderate value R1/R2 = 0.46/0.26 [15], where the near-threshold behavior of the cross-sections have been carefully taken into account. This choice is also supported by our results discussed later. Note that, in

[15], the product hydrogen in reaction R2 is given as H_2. This work remains an exception in this regard. We stick to 2H due to its wider acceptance in the literature (for example in [7, 31]).

Pressure and temperature dependence of selected reactions

In the following, our choice of the rate constants of R20-R25 is explained in detail.

$$Reaction\,(R20):\ SiH_4 + H \rightarrow SiH_3 + H_2$$

Magnitude at room temperature

There have been numerous experimental determinations of the rate constant k_{20}, all falling in the range between 2.1×10^{-13} and 8.5×10^{-12} cm^3/s at room temperature. The most recent determinations $(2.8 \pm 0.3) \times 10^{-13}$ cm^3/s [32] and $(3.38 \pm 0.16) \times 10^{-13}$ cm^3/s [20] at 298 K agree well with each other. Moreover, in [20] was stated a good agreement with the value averaged across the literature (to the exclusion of evident outliers) $(3.4 \pm 0.5) \times 10^{-13}$ cm^3/s, which seems to represent a well-established value at room temperature.

Temperature dependence

Being independent of pressure, the rate constant is sensitive to the temperature. This dependence was also measured in the two cited works. These data are in substantial agreement, showing only some divergence at the upper end of the temperature range. In view of this, the authors of [20] combine both datasets and provide a fit expression $(1.37 \pm 0.03) \times 10^{-10}$ exp[-(1820 ± 10)/T] cm^3/s for the temperature range 290–636 K. This temperature dependence is stronger than the expression cited in [7] 2.8×10^{-10} exp[-1250/T], giving discrepancies up to 40% in the range from 300 to 500 K. The latter expression is based on the results from [33], where the rate constant 4.3×10^{-13} was only measured at room temperature, after which the Arrhenius parameters were proposed relying on some 'admittedly crude approximation' according to the authors' words. Besides, in [14] was argued that this rate constant in a real SiH_4/H_2 plasma might be higher due to hot H atoms which are not fully thermalized after being produced by electron impact dissociation.

$$Reaction\,(R20):\ SiH_3 + H \rightarrow SiH_2 + H_2$$

Magnitude at room temperature

The values of the rate constant found in the literature range from 2×10^{-11} to 5×10^{-10} cm^3/s. In the analysis of a pulse radiolytic experiment [34], this constant was assumed 5×10^{-10} as a first approximation. Further, it was found that, divided by two, this value gives better agreement with the experimental data. The data was acquired at 300 K and in the atmospheric pressure range. In [3] a value of 10^{-10} was used. By modeling the results of their photolytic experiments [35], the authors inferred the rate constant $(2 \pm 1) \times 10^{-11}$ at 295 K and 9.5 Torr. Later, this value was quoted in [7]. However, in a later publication [8] with partly the same authors as in [7], a value of 5×10^{-10} was involved in their chemistry model. Simulation studies of another photolysis experiment in [20] yielded a value of $(4.3 \pm 1.0) \times 10^{-11}$ cm^3/s at 298 K and 500 Torr. Theoretical calculations [36] yielded 1.4×10^{-10} cm^3/s as association rate of $SiH_3 + H$ at 300 K.

T and p dependence

Ab initio theoretical calculations [37] demonstrated negligible pressure dependence (between 10^{-3} and 100 bar at least) and only slight temperature dependence in the range 300—2000 K. The Arrhenius expression 6.9×10^{11} $T^{0.736}$exp(134.8/T) $cm^3/mol/s$ yields 1.2×10^{-10} cm^3/s at room temperature. Somewhat higher value of 2.1×10^{-10} (T = 300 K) was obtained in another *ab initio* calculation study [21], that also confirmed missing pressure dependence in the range of interest and a weak temperature dependence. The interpolation expression for temperatures between 300 and 1000 K is 3.55×10^{-10} $T^{-0.05}$ exp(-77/T) cm^3/s. We opted for the rate constant from the latter work because it also provides a consistent set of rates for H-abstraction (R22 and R23) from other SiH_x radicals.

$$Reactions\,(R24—R25):\ SiH_2 + SiH_4 \rightarrow$$

This pathway is of utter importance for SiH_2 radical and for production of higher silanes. It has two channels [23]:

$$\rightarrow Si_2H_6 \quad (R24)$$

$$\rightarrow Si_2H_4 + H_2 \quad (R25)$$

While channel (R24) is strongly dominating at lower temperatures, channel (R25) gains in importance at higher temperatures due to the opposite trend in T dependence. The rate constant k_{25}(p,T) is given in figure 10(b) in [23]. At p = 1 Torr it can be well approximated by the following expression $k_{25}(T) = 5.15 \times 10^{-12}$ exp(-210/T).

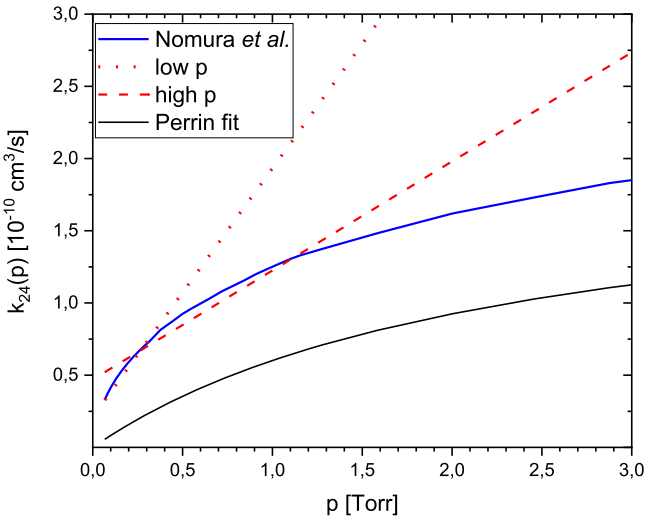

Figure 1. Rate constant for R24 found in [22] (blue solid line) and the two linear fits for different pressures (dotted and dashed lines), used in our model. Fit expression (solid black) by Perrin [7] based on the data from [38].

The pressure dependence is weak, and the rate constant may be considered pressure-independent in the temperature range where the contribution of this channel becomes significant.

Much more effort is needed to tackle the (R24) channel.

Experimental values at pressure about 1 Torr and at room temperature

In the pressure range of interest ($p < 1.5$ Torr) the rate constant k_{24} is in the fall-off regime, therefore, it depends on p and on the collision partner (buffer gas). Some experimental determinations at 1 Torr in helium buffer gas include $(6.7 \pm 0.7) \times 10^{-11}$ cm^3/s [38], 1.31×10^{-10} [39], 4×10^{-11} [40], $(1.1 \pm 0.2) \times 10^{-10}$ [41]. Later, the smaller values received criticism in [42]. In the present study, we regard values around 1.1–1.3 $\times 10^{-10}$ as the reference magnitude at room temperature. Data with different buffer gases can also be found in [42]. According to figures 3 and 4 of that study, the rate constant is about $(1.7 \pm 0.2) \times 10^{-10}$ in argon and 2.8×10^{-10} in SF_6. This trend is consistent with the concept that a heavier collision partner is more efficient in collisional stabilization of the intermediate complex. Furthermore, in [39] no significant difference has been observed at 5 Torr in helium buffer as compared with argon. In [43] no influence could be detected with argon addition to the SiH_4/H_2 mixture even at a much lower pressure of 9 Pa. On the other hand, in [22] somewhat lower values in helium than in argon (by a factor of ~1.5) have been determined below 1 Torr. This was explained by poor thermalization of SiH_2 radical in collisions with much lighter atoms.

T and p dependence

Channel (R24) features both pressure and temperature dependencies. The T dependence is quite strong: the value at 500 K is smaller by a factor of 6.7 than that at 300 K [23]. The p dependence is also substantial. The rate constant varies by a factor of ~3.0 between 0.1 and 1 Torr at 300 K and even stronger at 500 K. In the following, we explain how these values were derived.

The rate constant at various conditions was determined in a comprehensive experimental study [42], and its magnitude demonstrates an impressive agreement with the results of a later theoretical calculation [23] over the temperature and pressure range.

While the results presented in [23, 42] are for the pressure above 1 Torr, measurements in the pressure range $p < 1$ Torr at room temperature have been carried out in [22]. The determined rate constants and their pressure trend, given in figure 4 in that work, show a very good agreement with some earlier experimental results and with theoretical curve of [39]. This curve is reproduced in figure 1 as a blue line and is employed in our model as the reference dataset k_{24}(p,300 K). It amounts to 1.25×10^{-10} cm^3/s at the reference pressure 1 Torr.

To our knowledge, the only experimental determination of the rate constant at non-room temperature, besides the studies by Becerra [42], was reported in [43]. The measurement yielded $(2.3 \pm 0.5) \times 10^{-10}$ at 500 K and 9 Pa. This value, however, is rather close to the data at room temperature, cf figure 4 in [22].

Preparing expressions for Quantemol input

To handle the T dependence, the data from [23] (see figure 10(a) therein) was employed. The dataset k_{24}(p,300 K) was manipulated in order to generate smooth continuations to the curves at 500 K and 700 K.

Table 4. Coefficients for the approximation k(p,T) [cm^3/s] = $a_1(T) + a_2(T)^* p$[Torr], 300 K < T < 700 K. Within the indicated pressure ranges, the deviation remains less than 10% with respect to the reference curve k_{24}(p, 300 K) and to the datasets obtained for 500 K and 700 K by the procedure described in the text.

	a_1(T)	a_2(T)	Pressure range, Torr
Lower pressure	2.9×10^{-9} exp(-T/61)	1.25×10^{-8}(T/300)^{2}exp(-T/70)	0.05 < p < 0.4
Higher pressure	4.3×10^{-8}(T/300)^{4}exp(-T/44)	1.9×10^{-9}(T/300)exp(-T/93)	0.2 < p < 1.5

Since the pressure range is downside limited by 1 Torr, the data needs to be continued into the lower pressures. The pressure fits in [7] are based of the absolute values from [38, 40] which most likely underestimate the rate constant, as stated above. Multiplying by a factor of about 2.5, the absolute values can be adjusted to get the desired magnitude at 1 Torr. Even so, it seems problematic to use the resulting expressions at pressures below 1 Torr. The reference curve (blue line in figure 1) has a more convex shape in this pressure range. As a result, the rate constant is massively underestimated when using the fits by Perrin.

In order to generate input data for simulations with Quantemol software, the obtained datasets were fitted by expressions linear in p, in which case the reaction can be represented as a sum of binary and ternary processes. Since the datasets are strongly curved as functions of p, for each of the three temperatures two fit lines were produced: for a higher pressure and for a lower pressure range. The resulting coefficients are interpolated as functions of temperature, so that the rate constant takes the form $k(p,T) = a_1(T) + a_2(T) \times p$. This is shown in table 4.

Surface reactivities

To finalize the discussion on SiH_x chemistry, a few remarks are needed on the surface reactivities found in table 1. The values of β and s for SiH_3 are taken from [4]. The magnitude of the sticking coefficient for SiH_2 originates from an atomic-scale simulation study [10]. Therein, it was shown that the overall sticking coefficient for different H concentrations was approximately 70%. This value is close to the earlier estimates of 0.8 and also to an experimental determination 0.6 [43]. The sticking coefficient of the ions are taken as $s(SiH_x^+) = 1$, following the surface chemistry model presented in [6]. The ion-induced secondary emission coefficient was set to 0.033, as determined in [9].

Outline of Si_yH_x (y = 2, 3) plasma chemistry

In the literature, Si_2H_x radicals are less studied than SiH_x. What makes it more complicated is the fact that each Si_2H_x radical may exist in the form of different isomers with varied reactivities. Regarding Si_2H_4 radical, this is discussed in [14]. There is no way to do modelling without reasonable simplifying assumptions. Here we briefly describe our approach. The reasoning builds largely on results from [12]. Therein, three Si_2H_x radicals have been detected: Si_2H_2, Si_2H_4 and Si_2H_5. The fact that they survived in significant amounts on their way to the surface suggests that they might be represented by low-reactive isomers. Thus, our model assumes that all the three radicals exist in the form of low-reactive isomers. Specifically, this means that they do not react with the background gases SiH_4/H_2 and have moderate surface loss probability. Using the example of Si_2H_4 as discussed in [14], a highly-reactive form of this radical (silylsilylene) is produced in chemical reactions but then undergo a fast unimolecular isomerization towards a low-reactive form (disilene). In that study, the sticking coefficient for this isomer was assumed 0.4. In our model, we assume the surface loss probability $\beta(Si_2H_4) = 0.4$, and the sticking $s(Si_2H_4) = 0.1$. For Si_2H_5, the surface reactivities are assumed the same as for SiH_3. For Si_2H_2, we use $\beta(Si_2H_2) = 0.5$, as suggested in [12], and $s(Si_2H_5) = 0.1$ (0.3 was used in [12], but in their discussion the authors lean towards a lower value). Si_2H_3 radical was also included in our model, although in a highly reactive form only. It must be produced in R27 by substantial amounts, because SiH is a product of the primary dissociation. The data in [22] suggests that the rate constants of R27 and R24 are similar. On the other hand, high reactivity of Si_2H_3 results in enhanced consumption through R28 in the gas phase and high reactivity at the surface. Since Si_3H_x species are of minor relevance for the plasma-chemistry under present conditions, they are represented by a single lumped species. It effectively serves to close the system of rate equations for Si_1- and Si_2-chemistry. Within this lumped species, stable Si_3H_8 molecule has the most dominant contribution, with the radicals forming an insignificant part.

Computing with Quantemol software

Fluid simulations were performed using *Quantemol Virtual Tool* software [44]. This software package provides a GUI to the HPEM code developed by M Kushner [45]. It is capable of modelling 2D geometries with an option to choose either Cartesian or cylindrical coordinates. The mesh is defined in a way that all the numeric cells are the same and remain unchanged while simulation. The Boltzmann equation is solved for the electron energy

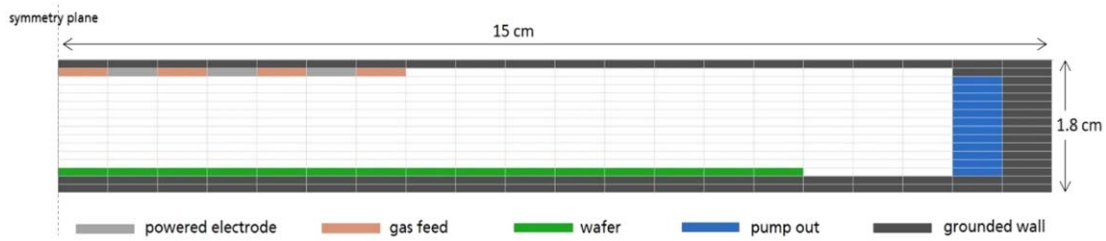

Figure 2. 2D simulation domain. The configuration of gas feed imitates a gas shower. Together with the grey cells they build up the powered electrode.

distribution function EEDF. It is then used to obtain the reaction rates for electron impact processes, listed in table 2. The time-dependent fluid equations are solved, whose solutions reach a steady state after a certain simulation time. It is these steady state values that we present and discuss in the following sections. The output of the model are the number densities, fluxes, and temperatures of the plasma species, as well as electric potential, consumed power, etc In the present study we discuss only capacitively coupled discharges at 13.56 MHz excitation frequency. The simulations were done with 10 MHz frequency though, because it is more practical to handle within the software.

Experiment

PECVD tool

Depositions of a:Si-H films have been performed using a capacitively coupled plasma (CCP) source which is part of the inline MAiA tool [46] manufactured by the company MeyerBurger. Its driving frequency is 13.56 MHz. The CCP source is rectangular in plane, of 12 cm length in transport direction and of 110 cm width. The discharge gap between the powered electrode and the carrier is about 1.2 cm. A gas mix of monosilane (SiH_4) and hydrogen (H_2) within a process pressure range of 0.1-0.4 Torr was applied. The deposited films have been analyzed by ellipsometry. In this study, only deposition at 0.225 Torr (30 Pa) has been used.

An example of 2D simulation mesh is shown in figure 2. This mesh was used to obtain results for case (3) when modelling MAiA CCP source.

Setup for the radio frequency discharge in [12]

Simulations for case (1) and case (2) are based on a mesh of a similar shape but different dimensioning. The 2D simulation domain was built following the brief outline of the geometric configuration found in [12]. It is characterized by a cylindrical symmetry with electrode radius 4.1 cm (diameter 8.2 cm) and substrate-to-electrode gap of 2 cm. The radical fluxes were calculated at the substrate center, corresponding to the centered position of the sampling orifice.

The radical densities at the substrate are calculated from the fluxes which were measured by TIMS (threshold ionization mass spectrometry) technique. The neutral radicals that pass through a small sampling orifice get ionized by electron impact. The use of near-threshold energy ensures that only the direct ionization occurs, i.e., each $Si_yH_x^+$ ion ($y = 0, 1, 2$) originates from the corresponding Si_yH_x radical. For the purposes of mass-resolved detection, the ions are further guided by the ion optics to the quadrupole mass spectrometer.

Results and discussion

Model validation at room temperature, cases (1) and (2)

For the purpose of testing the correctness of a plasma chemistry model, it is instructive to compare its predictions with experimentally measured densities of chemical species. Determination of many radicals simultaneously is rarely found in literature [8, 12]. For benchmarking, we have chosen work [12] which contains a comprehensive study of the whole set of SiH_x and Si_2H_x radicals at different discharge conditions. The experiments were carried out at room temperature at varying dilution ratio and pressure. We used these parameters as the input to our model and ran simulations with the respective geometric configuration.

In figure 3 and figure 4 we compare the radical densities of our simulations with those reported in table 1 of [12]. In that study, the densities were calculated from the measured surface fluxes. In our simulations, Quantemol software computes the fluxes onto the wafer as part of the output. Similarly, we use these fluxes to infer the densities. This is done in the following manner. The Quantemol algorithm considers two components

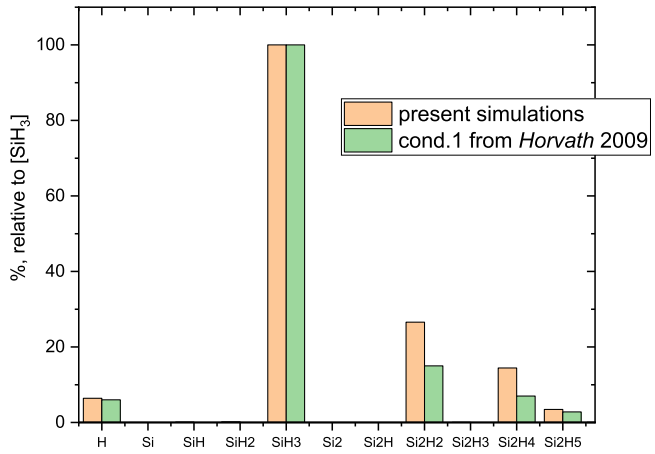

Figure 3. Number densities of the radicals near the substrate, $R_0 = 0$ (pure SiH_4), p = 0.3 Torr, T = 300 K. Shown are the densities from [12] that are above the sensitivity threshold. While all the simulated values are in the plot, some of them are so low that are not discernable on this scale.

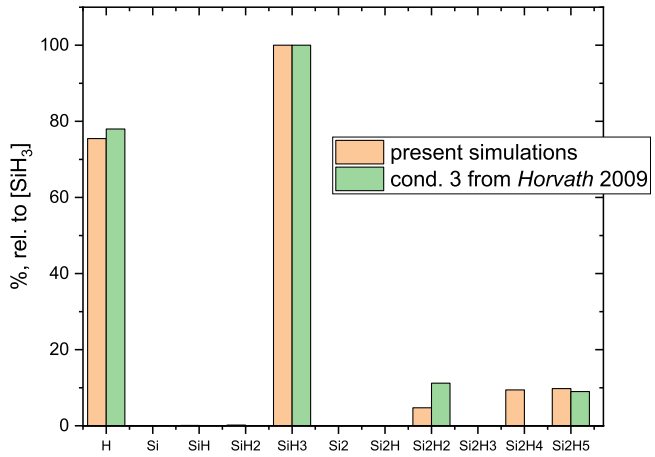

Figure 4. Number densities of the radicals at the substrate. $R_0 = 40$, p = 1.5 Torr, T = 300 K.

of a surface flux, the first one corresponding to the fluid average velocity, the second one arising from the thermal velocity of molecules. In our case, the latter component is largely predominant. Since we are interested in number densities, a ratio of fluxes times the inversed ratio of thermal velocities would yield the ratio of densities. Fluxes of all the radicals have been normalized to SiH_3 flux, making SiH_3 always appear as 100% on the diagram. Finally, they have been multiplied by the inversed ratio of thermal velocities, the velocity varying as $\sqrt{2T/m}$. At a common temperature T for all the radicals, the relative density of, say, atomic hydrogen is by a factor of $\sqrt{m_{SiH3}/m_H} \approx 5.6$ smaller than its relative flux.

The first column with results in table 1 of [12] was acquired in pure silane as feed gas (dilution ratio $R_0 = H_2 : SiH_4 = 0$), pressure of 0.3 Torr and room temperature. This is what we call case (1). These results are compared with our simulations in figure 3, the silane depletion was about 10% in both cases.

All in all, a good agreement can be stated. The ordering of the most abundant radicals is correctly reproduced and none of them is missing. While Si-containing radicals contribute to deposition, the role of H atom is the opposite, i.e., etching. Thus, for a correct prediction of the deposition rate, it is necessary to accurately account for H flux. Getting back to the discussion on the branching ratio of dissociation reactions R1/R2, it is noted that the value used in our model R1/R2 = 0.46/0.26 produces a relative H content that agrees very good to the findings of [12]. Whereas R1/R2 = 0.17/0.83 generates a large amount of excess H that cannot be dealt away, e.g., by assuming a higher surface loss probability β(H) which is already 1.0.

Figure 4 compares the data from the third column of table 1 of [12] with our simulations. This is case (2) of our validation. It corresponds to a condition of SiH_4 strongly diluted in H_2 with $R_0 = H_2 : SiH_4 = 40$. At elevated temperatures (200°C–250°C) characteristic of conventional PECVD deposition, the surface loss probability is β(H) ≈ 1. A reduction in β(H) on a growing a:Si-H surface is promoted by the combination of two factors (a)

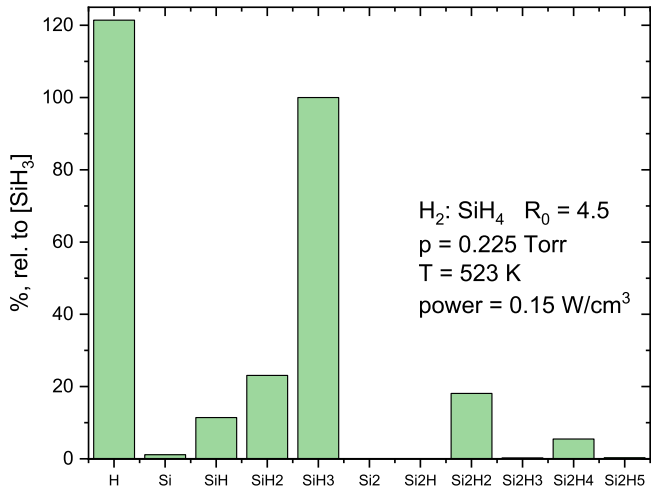

Figure 5. The radicals number densities. Bulk average values normalized to SiH_3 density of 4.2×10^{11} cm^{-3}.

lower temperature and (b) high dilution ratio [13]. Thus, from figure 5 in [13] we can deduce that $\beta(H) \approx 0.25$ for $R_0 = 40$. The value used in our simulation was $\beta(H)=0.4$, which gives better agreement than 0.3 or 0.5. Since the data represents the density near the surface, it is more sensitive to the loss probability than the average bulk value.

An interesting and novel result of the work by Horvath *et al* was eliciting a significant role of Si_2H_2 among the other Si_2H_x species. This radical is rarely included into plasma chemistry models, though. Meanwhile, the experimental data does not show Si_2H_4 radical. Most likely, its density lies slightly below the sensitivity threshold of 6%.

Model validation at T = 250 °C, case (3)

After validating the model at room temperature, we applied it to the MAiA capacitively coupled plasma source. Its model configuration is shown in figure 2. The x-dimension of 2D simulation domain was shorter than that of the real setup in order to save the computation time. We present the results for a typical set of parameters for PECVD depositions. The process temperature is around 250 °C, which is much higher than in cases (1) and (2) discussed above. A silane dilution of $R_0 = 4.5$ at total pressure p=0.225 Torr is applied. This is case (3) of our validation.

In contrast to the diagrams above, figure 5 shows the bulk average values, not the values at the surface in the center. A striking feature of these results is a high amount of hydrogen H. It is even larger than in case with $R_0 = 40$ (figure 4), which is counterintuitive. Two effects are responsible for this. Firstly, due to the difference in the surface loss probabilities of H and SiH_3, the proportion of H atoms would be lower if the densities at the surface were shown in figure 5 instead. Secondly, the surface losses of the atomic hydrogen are accompanied by enhanced volume losses in case of figure 4. This can be explained in the following way. H radical is produced by the electron-impact dissociation of SiH_4 as well as H_2 molecules. The losses are (a) due to the recombination on the surface and (b) due to H-abstraction reactions in the volume, most notably R20. The relative importance of volume/surface losses is characterized by the second Damköhler number (Da_{II}). Comparing the cases of figure 4 and figure 5, Da_{II} is estimated to be about 20 times larger in the first case, considering the differences in temperature, geometry, total and partial pressures and surface loss probability. This provides an indicator for the increased efficiency of the volumetric losses.

The relative number density of SiH_2 is higher than on the previous plots due to the temperature dependence of reaction R5, which leads to reduced losses of this radical at a higher temperature.

The resulting spatial distributions of plasma species typically show maximum in the region under the edge of the powered electrode. This is illustrated by a 2D mapping of SiH_3 radical in figure 6.

The indicated power density is reduced to the dimension of the powered electrode. In the simulation, the pumping residence time of a molecule was 0.3 s. This is close to the experimental value as estimated from the chamber dimensions, gas inflow and pumping. The residence time and the dissipated power determine the resulting gas depletion. With plasma on, SiH_4 density was only 24% of the initial plasma-off condition. Due to this high degree of depletion, the influent dilution ratio $R_0 = 4.5$ of the feed gases turns into the actual value $R = 22.2$ in the operated plasma chamber.

Silane is known to produce electronegative plasmas, i.e., large amounts of negative ions. In our case, the simulated number density of SiH_3^- is by a factor of 1.5 larger than electrons. The literature on experimental

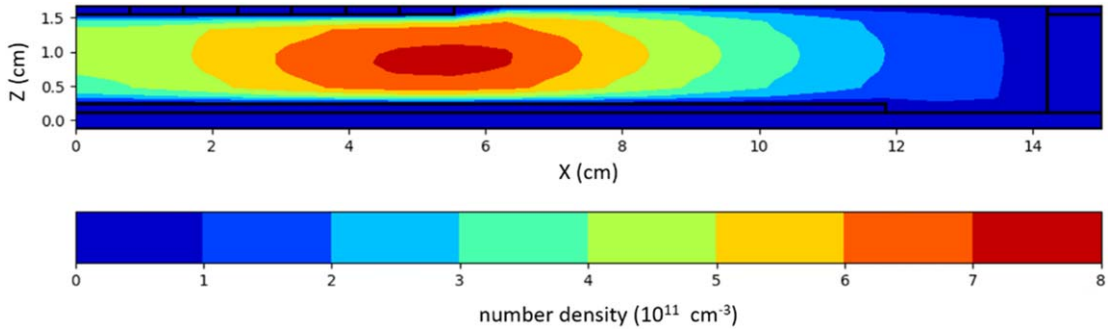

Figure 6. 2D mapping of SiH_3 simulated number density, $R_0 = 4.5$, p = 0.225 Torr, T = 523 K, dissipated power density 0.15 W cm^{-3}. Compare to figure 2 showing the basic mesh setup for the simulation.

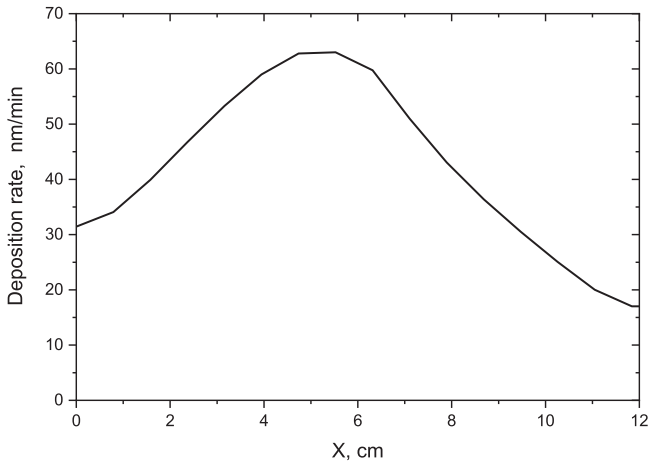

Figure 7. Simulated deposition rate on the wafer, 1D profile.

determination of electronegativity in silane-containing plasmas is scarce. Thus, in [47] the number density of the negative ions was estimated about 19 times larger than that of electrons for the case of $R_0 = 1$ dilution. In [48], with silane content of 0.5% (diluted in He) the densities of the negative ions and the electrons were found to be of comparable magnitude.

When modelling a real experimental situation, it has to be made sure that the dissipated power matches. Indeed, in both the experiment and the simulation the dissipated power density was around 0.15 W cm^{-3}. This value is reduced to the width of the powered electrode. An efficient path for power dissipation is the gas heating due to electron-impact rovibrational excitation. These reactions are not explicitly present in the plasma chemistry set. However, in Quantemol software, the power losses due to excitation of the four vibrational modes of SiH_4 molecule are automatically taken into account when solving Boltzmann equation. The problem of power dissipation in H_2/SiH_4 mixtures has also been tackled in [5]. The higher the H_2 content, the less efficient this dissipation channel is. From figure 3 in [5] we learn that, with actual R = 22.2, the power dissipated through this channel is about 12%.

The thickness of the deposited layer at this condition was measured by means of ellipsometry. It is about 18 nm for the inline process. Considering the speed of the tray 55 cm s^{-1} and the width of the plasma source about 12 cm, this thickness translates into deposition rate of $\approx$ 83 nm min^{-1}.

This value can be compared to the one obtained via simulation. The deposition rate profile is shown in figure 7. It was computed using the surface fluxes of radicals and ions and their sticking coefficients given in table 1. Also included is etching by H atoms, using the temperature-dependent expression for etch probability found in [8]. The non-uniform spatial profile of the deposition rate was averaged over the wafer, in the way like it is smoothed out by the inline motion of the carrier in the real setup. The resulting value of 40,6 nm min^{-1} was then reduced to the width of the powered electrode. This finally yields the deposition rate of 87 nm min^{-1}, which is in a very good agreement with the one from the experiment.

Conclusion

This paper presented work on the simulative representation of a PECVD process at radio frequency for the manufacturing of a-Si:H layers applying a gas mixture of monosilane and hydrogen. The model presented here includes some updated p and T dependencies of the rate constants and an advanced Si_2H_x chemistry. The simulations were run at various pressures p = 0.225, 0.3, and 1.5 Torr and two temperatures T = 300 K and 523 K. Overall, a good agreement can be stated by comparison with available benchmark data. A reduced surface loss of H atom was established in case of lower temperature and high dilution ratio. Also, the results strongly suggest that the branching ratio between dissociation channels R1 and R2 might be higher than the popular value 0.17/0.83.

The model is intended to examine the action of PECVD tools. A more detailed study on the MAiA CCP source will be presented in a coming paper.

Acknowledgments

This work was funded by the German federal ministry for economic affairs and energy under the project NextStep with the contract number 0324171B.

The authors would like to thank Jan Temmler, Leonard Kraus and Michael Hahn for their technical support and valuable discussions.

Data availability statement

All data that support the findings of this study are included within the article (and any supplementary files).

ORCID iDs

Vladimir Sushkov https://orcid.org/0000-0001-8136-4364

References

[1] Green M, Dunlop E, Hohl-Ebinger J, Yoshita M, Kopidakis N and Hao X 2021 *Prog. Photovolt. Res. Appl.* **29** 3
[2] Kushner M J 1987 *J. Appl. Phys.* **62** 2803
[3] Kushner M J 1988 *J. Appl. Phys.* **63** 2532
[4] Matsuda A, Nomoto K, Takeuchi Y, Suzuki A, Yuuki A and Perrin J 1990 *Surf. Sci.* **227** 50
[5] Perrin J 1993 *J. Phys. D: Appl. Phys.* **26** 1662
[6] Perrin J, Shiratani M, Kae-Nune P, Videlot H, Jolly J and Guillon J 1998 *Journal of Vacuum Science & Technology A: Vacuum, Surfaces, and Films* **16** 278
[7] Perrin J, Leroy O and Bordage M C 1996 *Contrib. Plasma Phys.* **36** 3
[8] Leroy O, Gousset G, Alves L L, Perrin J and Jolly J 1998 *Plasma Sources Sci. Technol.* **7** 348
[9] Böhm C, Perrin J and Roca i Cabarrocas P 1993 *J. Appl. Phys.* **73** 2578
[10] Ramalingam S, Mahalingam P, Aydil E S and Maroudas D 1999 *J. Appl. Phys.* **86** 5497
[11] Pandey S C, Singh T and Maroudas D 2009 *J. Chem. Phys.* **131** 34503
[12] Horvath P and Gallagher A 2009 *J. Appl. Phys.* **105** 13304
[13] Abe Y, Fukushima A, Takeda K, Kondo H, Ishikawa K, Sekine M and Hori M 2013 *J. Appl. Phys.* **113** 13303
[14] Amanatides E, Stamou S and Mataras D 2001 *J. Appl. Phys.* **90** 5786
[15] Janev R K and Reiter D 2003 *Contrib. Plasma Phys.* **43** 401
[16] 1987 *Swarm Studies and Inelastic Electron-Molecule Collisions* Pitchford L C *et al* (ed) (New York, NY: Springer) (*Proceedings of the Meeting of the Fourth International Swarm Seminar and the Inelastic Electron-Molecule Collisions Symposium, July 19–23, 1985, Tahoe City, California, USA*) 1st edn. (https://doi.org/10.1007/978-1-4612-4662-6)
[17] Janev R K, Langer W D, Post D E and Evans K 1987 *Elementary Processes in Hydrogen-Helium Plasmas: Cross sections and Reaction Rate Coefficients: Cross sections and Reaction Rate Coefficients* (Berlin, Heidelberg: Springer)
[18] Chan C F, Burrell C F and Cooper W S 1983 *J. Appl. Phys.* **54** 6119
[19] Gougousi T, Johnsen R and Golde M F 1995 *Int. J. Mass Spectrom. Ion Processes* **149-150** 131
[20] Arthur N L and Miles L A 1997 *Faraday Trans.* **93** 4259
[21] Raghunath P, Lee Y-M, Wu S-Y, Wu J-S and Lin M-C 2013 *Int. J. Quantum Chem.* **113** 1735
[22] Nomura H, Akimoto K, Kono A and Goto T 1995 *J. Phys. D: Appl. Phys.* **28** 1977
[23] Matsumoto K, Klippenstein S J, Tonokura K and Koshi M 2005 *The Journal of Physical Chemistry. A* **109** 4911
[24] Raghunath P and Lin M C 2013 *J. Phys. Chem.* A **117** 10811
[25] Baklanov A V and Krasnoperov L N 2001 *J. Phys. Chem. A* **105** 4917
[26] Zhang Q, Ru M, Wang M, Wang S and Gu Y 2001 *Sc. China Ser. B-Chem.* **44** 606
[27] Tanaka T, Hiramatsu M, Nawata M, Kono A and Goto T 1994 *J. Phys. D: Appl. Phys.* **27** 1660
[28] Janev R K, Reiter D and Samm U 2003 *Collision Processes in Low-Temperature Hydrogen Plasmas* (Jülich: Forschungszentrum Jülich)
[29] Allen W N, Cheng T M H and Lampe F W 1977 *J. Chem. Phys.* **66** 3371
[30] Perkins G G A, Austin E R and Lampe F W 1979 *J. Am. Chem. Soc.* **101** 1109

[31] Doyle J R, Doughty D A and Gallagher A 1990 *J. Appl. Phys.* **68** 4375
[32] Goumri A, Yuan W-J, Ding L, Shi Y and Marshall P 1993 *Chem. Phys.* **177** 233
[33] Austin E R and Lampe F W 1977 *J. Phys. Chem.* **81** 1134
[34] Mihelcic D, Schubert V, Schindler R N and Potzinger P 1977 *J. Phys. Chem.* **81** 1543
[35] Loh S K and Jasinski J M 1991 *J. Chem. Phys.* **95** 4914
[36] Takahashi J, Momose T and Shida T 1994 *BCSJ* **67** 74
[37] Barbato A, Seghi C and Cavallotti C 2009 *J. Chem. Phys.* **130** 74108
[38] Jasinski J M and Chu J O 1988 *J. Chem. Phys.* **88** 1678
[39] Baggott J E, Frey H M, Lightfoot P D, Walsh R and Watts I M 1990 *Faraday Trans.* **86** 27
[40] Dietrich T R, Chiussi S, Marek M, Roth A and Comes F J 1991 *J. Phys. Chem.* **95** 9302
[41] Inoue G and Suzuki M 1985 *Chem. Phys. Lett.* **122** 361
[42] Becerra R, Frey H M, Mason B P, Walsh R and Gordon M S 1995 *Faraday Trans.* **91** 2723
[43] Hertl M and Jolly J 2000 *J. Phys. D: Appl. Phys.* **33** 381
[44] 2023 Last checked 15.03.2023 (https://quantemol.com/software-2/quantemol-vt/)
[45] Kushner M J 2009 *J. Phys. D: Appl. Phys.* **42** 194013
[46] Bodlak L, Temmler J, Moldovan A and Rentsch J 2019 *AIP Conf. Proc.* **2147** 050001
[47] Tochikubo F, Suzuki A, Kakuta S, Terazono Y and Makabe T 1990 *J. Appl. Phys.* **68** 5532
[48] Shiratani M, Fukuzawa T, Eto K and Watanabe Y 1992 *Jpn. J. Appl. Phys.* **31** L1791–3